

**Emma J. D. Boland**

British Antarctic Survey

Cambridge, UK

March 7, 2023




Find attached a non-peer reviewed pre-print entitled *A Novel Heuristic Method for Detecting Overfit in Unsupervised Classification of Climate Models*. The authors are:

- Emma J. D. Boland, British Antarctic Survey, UK, [emmomp@bas.ac.uk](mailto:emmomp@bas.ac.uk), [@EmmaJDBoland](https://twitter.com/EmmaJDBoland)
- Erin Atkinson, University of Toronto, Canada, [erin.atkinson@mail.utoronto.ca](mailto:erin.atkinson@mail.utoronto.ca).
- Dani C. Jones, British Antarctic Survey, UK, [dannes@bas.ac.uk](mailto:dannes@bas.ac.uk), [@DaniJonesOcean](https://twitter.com/DaniJonesOcean)

This manuscript has been submitted to the journal *Environmental Data Science* for review.

RESEARCH ARTICLE

# A Novel Heuristic Method for Detecting Overfit in Unsupervised Classification of Climate Models

Emma J. D. Boland<sup>1</sup> , Erin Atkinson<sup>2</sup>  and Dan(i) C. Jones<sup>1</sup> 

<sup>1</sup>British Antarctic Survey, Cambridge, CB3 0ET, United Kingdom

<sup>2</sup>Department of Physics, University of Toronto, Toronto, M5S 1A7, Canada

Received xx xxx xxxx

**Keywords:** Climate Modelling, Unsupervised Classification, Methods, Ocean Data

## Abstract

Unsupervised classification is becoming an increasingly common method to objectively identify coherent structures within both observed and modelled climate data. However, in most applications using this method, the user must choose the number of classes into which the data are to be sorted in advance. Typically, a combination of statistical methods and expertise is used to choose the appropriate number of classes for a given study, however it may not be possible to identify a single ‘optimal’ number of classes. In this work, we present a heuristic method, the Ensemble Difference Criterion, for determining the maximum number of classes unambiguously for modelled data where more than one ensemble member is available. This method requires robustness in the class definition between simulated ensembles of the system of interest. For demonstration, we apply this to the clustering of Southern Ocean potential temperatures in a CMIP6 climate model, and show that the data supports between four and seven classes of a Gaussian Mixture Model.

## Impact Statement

One method that climate scientists use to find structures in environmental data is unsupervised classification, where a machine learning model sorts data, such as temperatures from different parts of the ocean, into groups or classes. This paper proposes a new way of determining if an unsupervised classification model has ‘over-fit’ the data available, which means it is using too many classes. This method will be useful for climate scientists using unsupervised classification for studying climate models, as current criteria commonly used often don’t provide an upper limit on the number of classes.

## 1. Introduction

Studies using observational data of the climate system often seek to find structures within that data. Specifically, classifying complex data into coherent groups with similar properties is often the first step in a study that may seek to, for example, find borders between groups, describe the behaviour of each group, explain the differences between the groups, or track changes in groups over time.

Unsupervised classification methods, i.e. methods that do not know a-priori what the properties of these groups might be, have proven adept at identifying coherent spatial structures within climate data, even when no spatial information is supplied to the algorithm. In studies of ocean and atmospheric data, two commonly used unsupervised classification methods are k-means (Liu et al., 2021; Houghton

and Wilson, 2020; Yuchechen et al., 2020; Hjelmervik et al., 2015; Hjelmervik and Hjelmervik, 2014, 2013; Solidoro et al., 2007; Sonnewald et al., 2019) and Gaussian mixture modelling (GMM) (Fahrin et al., 2022; Sugiura, 2021; Zhao et al., 2021; Crawford, 2020; Jones et al., 2019; Maze et al., 2017a; Tandeo et al., 2014; Hannachi, 2007; Hannachi and O’Neill, 2001). K-means attempts to find coherent groups by "cutting" the abstract feature space using hyperplanes, whereas GMM attempts to represent the underlying covariance structure in abstract feature space using a linear combination of multi-dimensional Gaussian functions.

However, when dealing with highly-correlated data such as oceanographic model output, the number of classes into which the data should be divided is not necessarily obvious; it remains a relatively unconstrained free parameter, and the classification methods themselves do not typically provide a way of choosing the ‘best’ or most appropriate number of classes to describe a given dataset. In practice, most studies repeat the training of the model multiple times for different numbers of classes before applying a statistical criterion to compare the models. Statistical criteria alone do not always show a clear single ‘best’ model, and so domain expertise is often additionally used to determine the appropriate number of classes for a given study.

The most commonly used statistical criterion is the minimum in the Bayesian Information Criterion (BIC, Schwarz, 1978), used in Fahrin et al. (2022); Sugiura (2021); Zhao et al. (2021); Jones et al. (2019); Maze et al. (2017b); Hjelmervik et al. (2015); Hjelmervik and Hjelmervik (2014, 2013); Sonnewald et al. (2019). The BIC is comprised of two terms: a term that rewards the statistical likelihood of the model and a term that penalises overfitting. One looks for a minimum or plateau in BIC in order to find the number of classes that maximises statistical likelihood without overfitting.

Other common statistical methods used to compare clustering results by class number include the following (a non-exhaustive list):

- Akaike Information Criterion (AIC, Akaike, 1973), used in Tandeo et al. (2014); Sonnewald et al. (2019),
- Caliński–Harabasz criterion (CHC, Caliński and Harabasz, 1974), used in Yuchechen et al. (2020),
- Davies-Bouldin index (DBI, Davies and Bouldin, 1979), used in Solidoro et al. (2007),
- Silhouette coefficient (Rousseeuw, 1987), used in Houghton and Wilson (2020),
- criteria based on confidence intervals, used in Hannachi (2007).
- other scores based on log-likelihoods, used in Hannachi and O’Neill (2001); Crawford (2020),

Studies such as Liu et al. (2021) use physical justifications only.

Most of the studies cited above use unsupervised classification on observational data. One natural extension of a study based on observational data is to carry out a similar study based on data from numerical simulations. This allows one to assess the model’s fidelity, as well as greatly expanding the scope of the questions that can be asked, such as how robust clustering results are between different ensemble members, and how cluster properties vary in different modelling scenarios.

In this study, we describe the results of the unsupervised classification of Southern Ocean temperature profiles from a CMIP6 model using a Gaussian Mixture Model (GMM). We first describe the dataset and classification model in section 2.1. In section 3 we present the results of an eight class model and compare them with the results of Jones et al. (2019), which is based on observations of the Southern Oceans from the Argo float network.

In section 4 we compare a number of criteria for determining the optimal number of classes, including the novel Ensemble Difference Criterion, which is a novel heuristic method for determining the maximum number of classes when classifying multi-member ensembles of climate model data. We discuss how to interpret the results of the different criteria in section 5 and finish in section 6 with a summary.

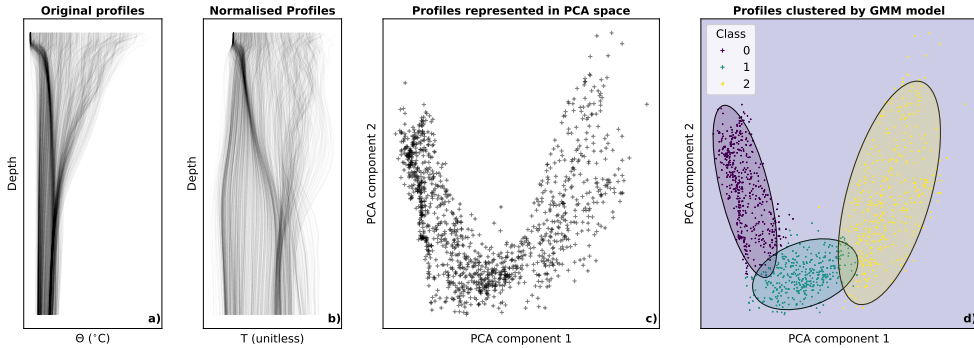


**Figure 1.** An overview of the classification process using 1200 random Southern Ocean profiles from the year 2000. Raw profiles (a), are normalised (b) so each depth level has a mean of zero and a standard deviation of one. c) The profiles are transformed into PCA space. Two PCs are shown here; each point corresponds to one temperature profile. d) The data are classified according to a GMM. Three components are chosen in this figure, with an equi-probability surface shown for each, separately.

## 2. Data and methods

This section is arranged as follows: firstly, we describe the dataset of temperature profiles from the UK-ESM CMIP6 simulations (section 2.1), then we describe the form of the GMMs we fit to those data (section 2.2).

### 2.1. The dataset

The simulation dataset is the ocean potential temperature data from the historical (1850-2014) UK-ESM1.0 contribution to CMIP6 (Sellar et al., 2019). Ten ensembles were included, those with realisation number r1 through r10. A description of the UK-ESM variant-IDs can be found in <https://ukesm.ac.uk/cmip6/variant-id/>. Each ensemble represents a different run or *realisation* of the Earth's climate system.

We take data from 2001-2017 inclusive (17 years) in order to allow comparison with Jones et al. (2019) who use the same time period. As in Jones et al. (2019), we use ocean potential temperature-depth profiles south of 30°S that extend to at least 2000m. The dataset is thus a set of  $N$  vectors  $\{\mathbf{T}_i\}$ , one for each surface grid cell that fits the above criteria.

This results in a total of approximately 4.5 million profiles. We use a subset of 3,000 randomly chosen profiles per month, a total of 612 thousand profiles (13.5% of the full dataset), to train the model, then classify all profiles.

### 2.2. Classification scheme

Figure 1 gives an overview of the classification process. As an initial step, the raw dataset is normalised so that each depth level has mean zero and standard deviation one.

Each profile is  $L = 30$ -dimensional (determined by the number of depth levels between 100m and 2km in the model). The large number of dimensions makes computation expensive and hinders the usefulness of distance metrics on the normalised dataset. Principal component analysis (PCA) (Abdi and Williams, 2010) is employed as a dimensionality-reduction step. The dataset in PCA space is given by:

$$\mathbf{x}_i = \mathbf{P}\mathbf{T}_i, \quad (1)$$

where  $\mathbf{x}_i$  are the principal components representing the profile  $i$  and  $\mathbf{P}$  is the projection matrix. In the following analysis,  $M = 3$  principal components are used - the first three PCs are sufficient to explain 99.8% of the variance in the training dataset.



The training dataset is fitted to a Gaussian mixture model (GMM) (Anderson and Moore, 2012) as in Jones et al. (2019). This assumes that the data points  $\mathbf{x}_i$  are sampled from a joint distribution over profiles  $\mathbf{x}$  and class  $k$  (a *Gaussian mixture*), with probability

$$\rho_k(\mathbf{x}) = \lambda_k \mathcal{N}(\mathbf{x}; \boldsymbol{\mu}_k, \boldsymbol{\Sigma}_k), \quad (2)$$

where

$$\mathcal{N}(\mathbf{x}; \boldsymbol{\mu}_k, \boldsymbol{\Sigma}_k) = \frac{1}{\sqrt{(2\pi)^M |\boldsymbol{\Sigma}_k|}} \exp \left[ -\frac{1}{2} (\mathbf{x} - \boldsymbol{\mu}_k)^T \boldsymbol{\Sigma}_k^{-1} (\mathbf{x} - \boldsymbol{\mu}_k) \right] \quad (3)$$

is a multivariate Gaussian distribution with mean  $\boldsymbol{\mu}_k$  and covariance matrix  $\boldsymbol{\Sigma}_k$ , and

$$\lambda_k \in [0, 1], \sum_{k=1}^K \lambda_k = 1 \quad (4)$$

is any distribution over the set  $\{k_i\} = [1, K]$  where  $K$  is the total number of classes. The marginal distribution of the profiles  $\mathbf{x}$  is

$$\rho(\mathbf{x}) = \sum_{k=1}^K \rho_k(\mathbf{x}). \quad (5)$$

This work uses the GMM classification model from the `scikit-learn` Python package (Pedregosa et al., 2011). This implements an expectation-maximisation algorithm to learn the set of parameters  $\{\lambda_k, \boldsymbol{\mu}_k, \boldsymbol{\Sigma}_k\}$  from the training dataset. Each data point is then assigned to a single class according to the Gaussian distribution it most likely belongs to, i.e. the class with the greatest probability  $\rho_k(\mathbf{x}_i)$ :

$$k_i = \arg \max_k \rho_k(\mathbf{x}_i). \quad (6)$$

The final result of the classification is a function that maps from a temperature profile to a class index, which is used to classify the full dataset, including the training data:

$$f : \mathbf{T}_i \mapsto k_i, \quad (7)$$

as well as providing the probability distributions  $\rho_k$ . This allows one to define the overall certainty of the model as the sum of the log-likelihoods  $\mathcal{L}(K)$ :

$$\mathcal{L}(K) = \sum_i^N \log(\rho(\mathbf{x}_i)), \quad (8)$$

which is a measure of how well a given GMM represents the data.

### 3. Comparison with Observations

We first compare an eight-class GMM fit on the model data, as described in section 2, with the results of Jones et al. (2019), who fit an eight class GMM on Argo data from the same time period. We present this in order to provide the context for discussing the choice of class number in section 4, and leave detailed discussion of the physical interpretation of these results to another study.

Figure 2a) shows the ensemble mode (i.e. most common) class for each point in the domain, across the dataset time period (2001-2017) and all ten ensemble members (which are shown individually in the supplementary information, figure S1). For each ensemble member, the classes are first sorted from coldest to warmest by the average profile temperature value at the shallowest level (5m). Note that, for

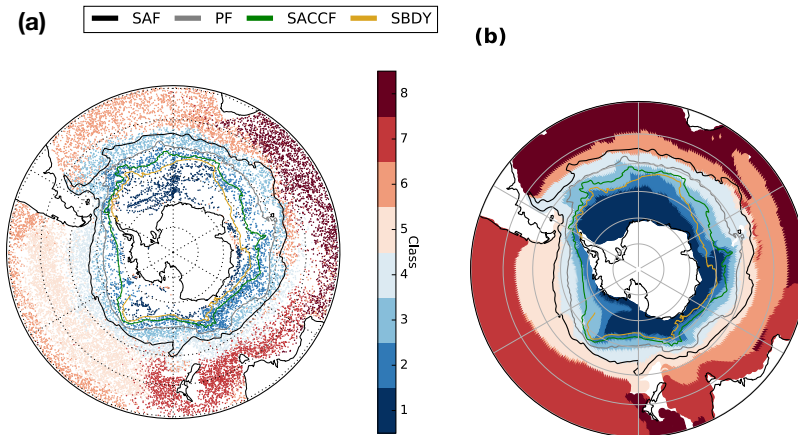


**Figure 2.** Comparison of the class assignments from Argo (a, Jones et al., 2019) and the ensemble mode class from UK-ESM (b), for 2001-2017. See text for further details. The ocean fronts from Kim and Orsi (2014) are marked by the coloured lines as labelled.

eight classes, this does not always result in alignment between the classes that are most similar to one another, see figure 7 and the discussion in section 4.

Despite this, there is relatively little inter-ensemble variation in the mean temperature profiles for the classes sorted in this manner: figure 3b) shows the ensemble and time mean profiles (solid lines), with the standard deviations of the time mean profiles from each ensemble (dotted lines) smaller than the ensemble mean of the temporal standard deviations (dashed lines). For comparison, figure 3a) shows the mean and standard deviations of the temperature profiles from Jones et al. (2019), sorted by the shallowest temperature.

Comparing the mean profiles between the two observationally-derived GMM and the model-derived GMM using the mean Euclidean distance in temperature/depth space (see section 4 for more details), we can map from each class in one model to the class it is most similar to in the other model (blue and red arrows in figure 3).

The two GMMs show some structural similarities with the coldest four classes (1-4) largely being circumpolar, with boundaries somewhat aligned with the climatological ACC fronts. The warmer classes (5-8) show a more basin dominated structure in both models. There are, however, differences in the detailed structures: within the Southern Boundary (yellow line) the UK-ESM model has two distinct classes, 1 and 2, whereas the Argo model has only one (class 1). This could be due to the extreme sparsity of Argo data here, as well as the fact it is likely to be from Austral summer only (when the region is ice-free), whereas the UK-ESM data is year-round.

Both models then have two circumpolar classes that lie roughly between the Southern Boundary and the SAF - class 3 & 4 in UK-ESM and 2 & 3 in Argo, with mean profiles that match well (see arrows in figure 3). Both class 5 in UK-ESM and Class 4 in Argo extend in a roughly zonal band from the South West coast of South America westward to the south Indian ocean, and show similar mean profiles. This suggests the structure of the ACC is a strong bound on the water properties, producing similar class boundaries in physical space and similar mean profiles in both models.

The geographic distributions of the warmest classes is most different between the two models, with classes 5 to 8 in the Argo model mostly confined to a single basin or sub-region. The three sub-tropical class in the UK-ESM model show a more cross-basin structure. This could be because there are fewer sub-tropical classes in the UK-ESM model than the Argo model, (three vs four). This can be tested by increasing the number of classes in the UK-ESM model to nine. This does lead to an extra sub-tropical

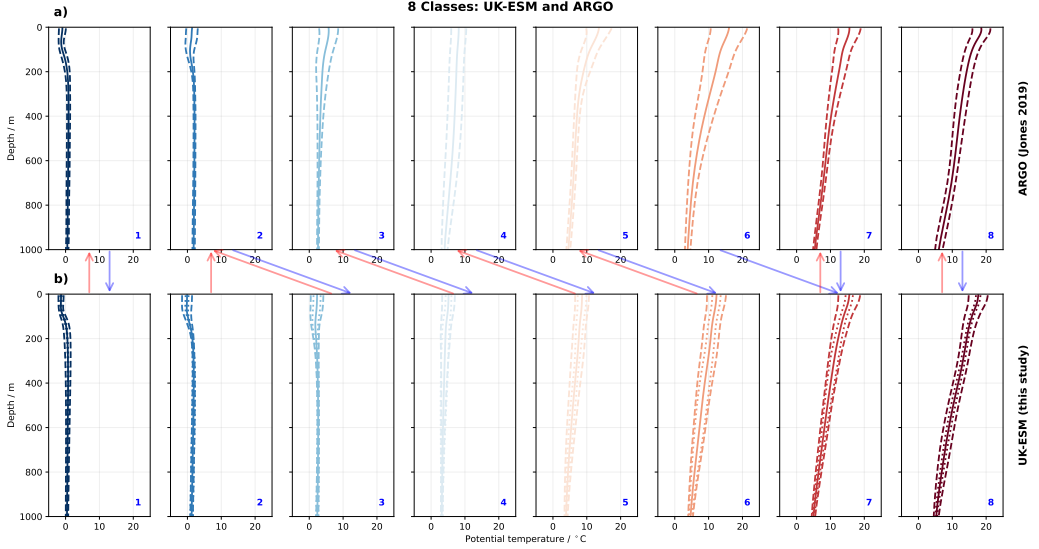


**Figure 3.** The mean temperature profiles for an 8 class GMM from *Jones et al. (2019)* (a) compared with the ensemble mean profiles from this study (b). Dashed lines indicate the standard deviation across samples for the Argo data, and the ensemble average of the temporal standard deviations for the UK-ESM data. The dotted line indicates the ensemble standard deviation in the temporal mean profiles for the UK-ESM data. Red arrows indicate the mapping from a UK-ESM class to the closest class in the Argo data, and the blue arrows indicate the same for the Argo classes and the closest classes in the UK-ESM data.

class in the model, but the structure is no more similar to the Argo data than for the eight class model (see figures S2 in the supplementary info).

The difference in structures of the sub-tropical classes between the two models could also be because the temperature profiles in this region are too similar to cluster well. This is indicated by the very similar structure of the warmest mean profiles in figure 3, and may indicate that the datasets do not robustly support eight unique classes. A comparison of various methods to find a robust choice of classes is carried out in the next section.

## 4. Choosing the number of classes

The key free parameter in the fitting of a GMM is the total number of classes  $K$ . Choosing a value of  $K$  presents a trade-off: low values will exhibit fewer structures and may fail to capture some of the underlying covariance structure whereas high values risk overfitting, losing physical interpretability and predictability. We here describe in more detail three criteria that we will use to analyse our results: the Bayesian Information Criterion (BIC), the silhouette coefficient, and a novel method, the Ensemble Difference Criterion (EDC).

### 4.1. Bayesian information criterion

#### 4.1.1. BIC: Definition

The BIC is a cost metric that rewards a high total likelihood of the data  $\mathcal{L}(K)$ , while regularising based on the estimated number of free parameters in the GMM  $N_f(K)$ . The AIC is similarly defined but

weights the number of parameters differently:

$$\text{BIC}(K) = -2\mathcal{L}(K) + N_f(K) \ln(N), \quad (9)$$

$$\text{AIC}(K) = -2\mathcal{L}(K) + 2N_f(K), \quad (10)$$

$$N_f(K) = K - 1 + KM + \frac{1}{2}KM(M - 1). \quad (11)$$

For this study, the BIC and AIC were almost identical for all clustering models studied, indicating the dominance of the log-likelihood term over the free-parameter terms in equations 9 and 10. Thus from now on we will only refer to the BIC.

A low BIC implies that the model fits the data well, while also avoiding overfitting. An optimal value of  $K$  can be determined by, for example, a minimum in the BIC curve, or for a value of  $K$  above which there are diminishing returns, determined by looking at the  $\Delta\text{BIC}$  curve, that is the change in score for adding an extra class.

#### 4.1.2. BIC: Results

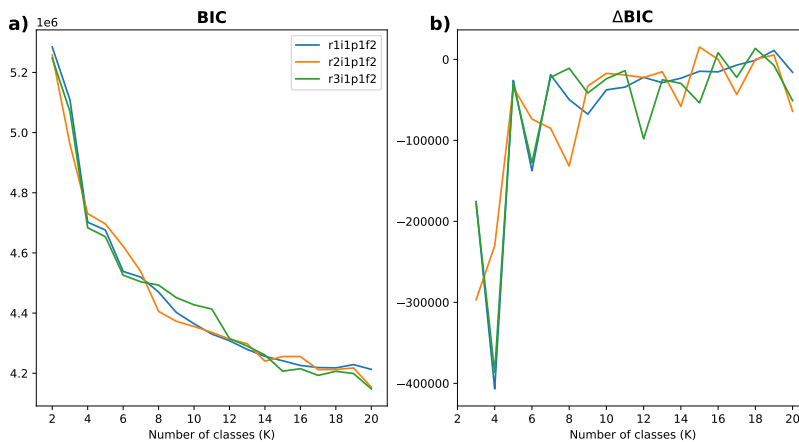


**Figure 4.** The a) BIC curves and b)  $\Delta\text{BIC}$  curves for three of the ensembles.

The BIC and  $\Delta\text{BIC}$  curves for three ensemble members, clustered into a range of class numbers, as described in section 2.2, is shown in figure 4. There is no clear minimum in the BIC curve (figure 4a) for up to 20 classes, so no clearly optimal value of  $K$ . The  $\Delta\text{BIC}$  curve (figure 4b) shows that adding an extra class leads to the largest improvements for 3 and 4 classes, then the gains begin to diminish for  $> 5$  classes. However, there is large variability between and within ensemble members, and some class values lead to an *increase* in the BIC for a given ensemble member.

## 4.2. Silhouette coefficient

### 4.2.1. Silhouette coefficient: definition

The silhouette coefficient is a measure of how well the clusters in a model are separated from each other. For each classified sample, the sample silhouette coefficient  $S_i$  is based on comparing the mean separation of the sample from all samples in the same class ( $a_i$ ) and the mean separation of the sample

from all samples in the next nearest class ( $b_i$ ):

$$S_i = \frac{b_i - a_i}{\max(a_i, b_i)}. \quad (12)$$

Note that in our example, the distance is defined between samples is calculated in PCA space, the space on which the samples are classified (see figure 1d), and not in geographical space.

$S_i$  can vary from -1 (a ‘poor’ score, indicating the sample is closer to samples in the neighbouring class than its own) to 1 (a ‘good’ score, indicating the sample is far from samples in the neighbouring class), whereas a score of 0 indicates overlapping classes. The overall silhouette coefficient for a given model is the mean of the sample silhouettes, i.e.  $SIL \equiv 1/N \sum_i^N S_i$ . Maximising the silhouette coefficient therefore desirable for applications where well-separated classes is a priority.

#### 4.2.2. Silhouette coefficient: Results

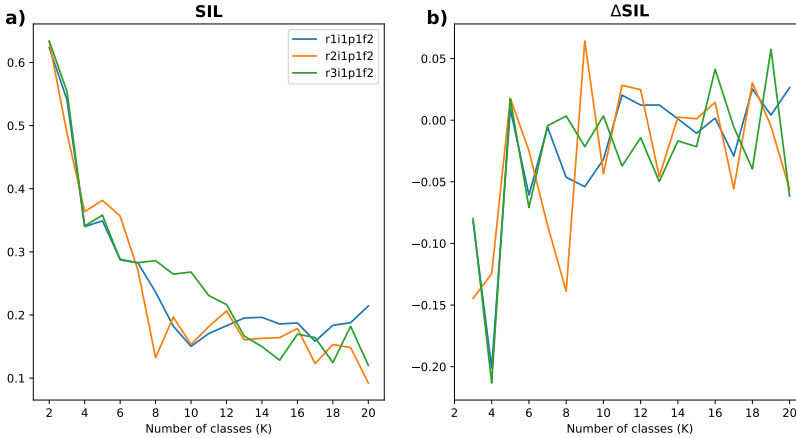


**Figure 5.** The a) SIL curves and b)  $\Delta$ SIL curves for three of the ensembles.

The SIL and  $\Delta$ SIL curves for three ensemble members, clustered into a range of class numbers, as described in section 2.2, are shown in figure 5. For each ensemble member, we calculate the SIL for a random subset of 10,000 samples (approx 1.6%) from the training set, due to the computational intensity of the calculation. Conversely to the BIC (section 4.1), it is desirable to *maximise* the SIL score.

The overall maximum SIL is for two classes, and there appears to be a local maximum at five classes for the three ensembles shown. As with the BIC, there is large variability both between and within ensemble members, especially at higher numbers of classes.

### 4.3. Ensemble Difference Criterion

If multiple realisations of the dataset are available, for example the ten historical ensemble members of UK-ESM, the simulated data can be leveraged to determine a physically-motivated and unambiguous value of the maximum number of classes.

#### 4.3.1. EDC: Definition

Firstly we define a map between class indices in different ensembles

$$f^{E_1 \rightarrow E_2}(k) = \arg \min_l \|\mathbf{T}_k^{E_1} - \mathbf{T}_l^{E_2}\|^2, \quad (13)$$

where  $\mathbf{T}_i^{E_j}$  is the mean temperature profile of the  $i$ th class in ensemble  $E_j$ , such that  $f^{E_1 \rightarrow E_2}(k)$  is the index of the class in ensemble  $E_2$  that is most similar to the class with index  $k$  in ensemble  $E_1$ .

Here ‘most similar’ is defined as the profile that minimises the Euclidean distance in temperature/depth space, but the method is not dependent on this exact choice as long as it allows one to identify correspondences between classes from different GMMs. Other maps could include, for example, the Euclidean distance between class centres in PCA space, the variance of each depth level, or the mean temperature of each class. We tested calculating the Euclidean distances in PCA space for the results reported here (in sections 3 and 4.3.2), and most mappings were identical to those using temperature/depth space, with occasional differences for one class in a given ensemble member (not shown).

If the map between class indices is not bijective, i.e. more there are classes that are matched with more than one other class, (e.g. figure 7) then the GMM, with this number of classes, can be rejected.

The number of classes is thus chosen based on a robustness criterion: if the differences between the average profiles within an ensemble is similar to, or less than, the differences between classes from different ensemble members, then the results are not robust and the model is rejected. Put conversely, we expect the class definitions to be robust across ensemble members for the GMM to be acceptable. We will refer to this as the Ensemble Difference Criterion (EDC).

#### 4.3.2. EDC: Results

An example of using the EDC for the UK-ESM data is shown in figures 6 and 7. Figure 6 shows an example of matching between 7-class GMMs fit to two ensemble members. The matching is successful because the map is bijective for all ensemble pairs (only one is shown here): each class in one model is matched by only one class in any other model.

Figure 7 shows an example of matching between 8-class GMMs to the same two ensemble members. The matching is not bijective in this case. For example, classes 6 and 7 in the r1i1p1f2 model are both closer to class 2 in the r2i1p1f2 model than to any other. The mapping fails for all pairs between the ten ensembles (only one is shown here), with some mappings finding three classes match to the same referent.

Thus, for this training set and 8-class GMM, the variation between ensembles is greater than the variation between classes within an ensemble, and hence the classes are not consistent across realisations of the system so the learned model is rejected. The EDC in thus chooses 7 classes as the maximum number for this training set.

## 5. Discussion

The lack of a clear optimal number of classes from any of the methods tested is perhaps expected, the ocean is a complex system and the GMM representation of the covariance structure in abstract feature space will always be an approximation. Rather, the number of classes will be chosen based on what produces a physically reasonable, and practically useful, distribution. This cannot be determined by statistical tests alone and indeed, in other clustering work, tests such as BIC are accompanied by simply plotting the class distribution for different values of  $K$  and determining which is most reasonable, as well as investigating the dependence of the results on the number of classes (see, for example, Jones et al., 2019; Houghton and Wilson, 2020). This is typically sufficient; however it may be antithetic to the motivation for automatic clustering in this application, where the identification of different classes is to be performed without the influence of previous clustering studies.

In our particular use case, we are attempting to classify bodies of water that are geographically and physically linked across a range of spatial and temporal scales, and so we do not expect exact separation

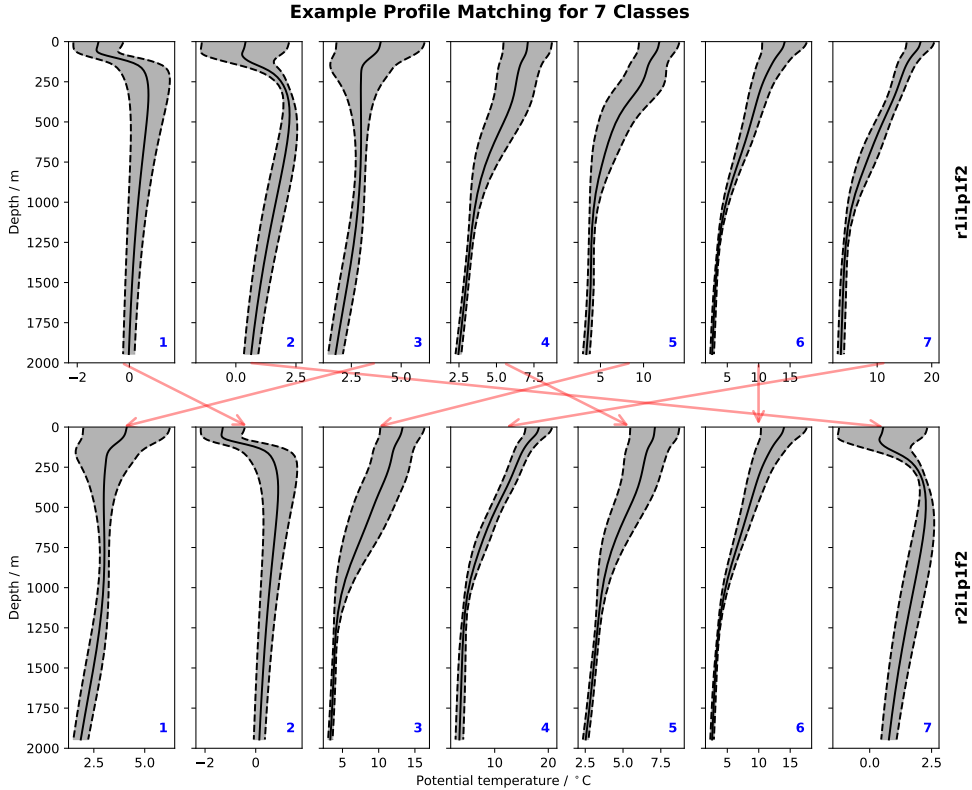


**Figure 6.** An example of using the Ensemble Difference Criterion (EDC) to match classes resulting from a 7-class GMM of two different ensemble members (*r1i1p1f2* and *r2i1p1f2*).

between classes, but rather expect a degree of overlap between classes. Indeed, this is why the GMM is chosen, which explicitly allows for such overlap. The nature of the GMM also allows for classes that may be very different shapes and sizes in PCA space. This means that metrics such as the SIL may not be ideal for assessing a GMM, as having a tightly shaped class neighbouring a broader class will give a relatively low SIL for the broader class, when in fact the model is a ‘good’ fit by other measures. Thus we believe the SIL is a less fitting metric than scores based on the overall likelihood (BIC/AIC) for our application, but it nonetheless helps by providing complementary information.

Comparing the SIL and BIC, we can see a trade-off between worsening class separation and increased likelihood, as indicated by decreasing SIL and BIC with increasing class number  $K$ . The BIC or AIC would seem to be better metrics for this application as they are designed to balance goodness of fit with a penalty for over-fitting. However, we did not see any difference between the BIC and AIC scores for the models we generated, implying that the over-fitting penalty is very small at these number of classes. This essentially means the BIC and AIC do not provide an upper limit on the number of classes in this case, as the over-fitting penalty is much smaller than the likelihood factor for the models studied here. This plateauing of the BIC and AIC is also seen in, for example, [Sonnewald et al. \(2019\)](#).

The physical motivation of the EDC scheme is advantageous over purely statistical tests such as BIC. However, there are two caveats to the EDC that should be highlighted. Firstly, using it assumes that, for the time period sampled, we should expect the Southern Ocean in each ensemble to be in comparable conditions. This need not be true, if, for example, they are in different phases of the SAM or ENSO. Secondly, in effect all this method has done is move the ambiguity in the process from the

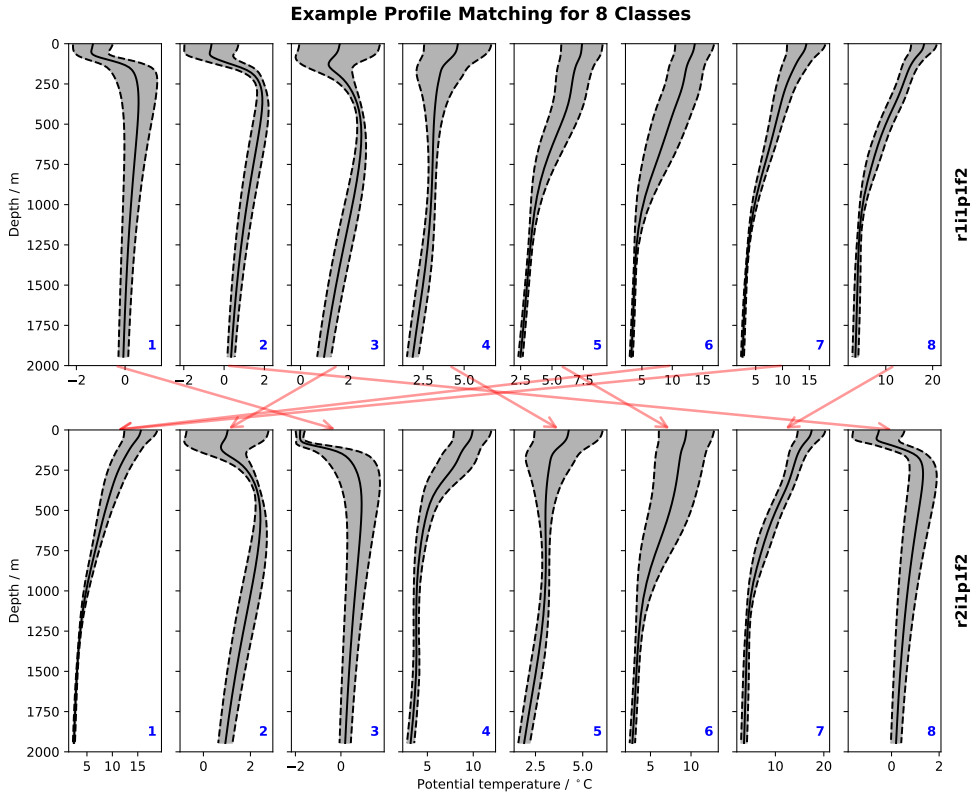


**Figure 7.** An example of using the Ensemble Difference Criterion (EDC) to match classes resulting from a 8-class GMM of two different ensemble members (*r1i1p1f2* and *r2i1p1f2*). Note that the map between classes of each ensemble is not bijective - 6 and 7 in the first ensemble are both matched to class 2 in the second.

specific choice of cost metric used, and subsequent method of choosing a minimum, to the choice of the how to determine the correspondence between classes in each ensemble.

Given the limitations of all the criteria discussed, the best estimate of the number of classes may come from trying to combine the information from all three (the BIC, the SIL and the EDC). The SIL score prefers 2 or 5 classes, depending on the absolute or local maximum, the BIC curve points to 4 or more classes, and we can use the EDC to provide an upper limit of 7 classes for our models, resulting in an overall range of 4 to 7 classes supported by our analysis.

## 6. Summary

Unsupervised classification studies are becoming increasingly common in the study of observed and simulated climate data. In many cases, techniques such as Gaussian Mixture Models (GMMs) and K-means clustering have been remarkably successful at identifying structures that are coherent in time and space, despite not being provided with temporal or spatial information. The property driven-approach of these methods is attractive when the aim is to objectively identify structures. That is not to say that domain knowledge is un-necessary, and in fact experience of the climate system is required to interpret the results and place them in context.

Unsupervised classification methods generally require no external input beyond the data, and the number of classes into which the data should be divided. However, there is not necessarily an obvious



choice for this number, which is a relatively unconstrained free parameter. In practice, most studies use statistical criteria such as the Bayesian Information Criterion (BIC) or Silhouette score to compare the results of training the model multiple times for a range of number of classes.

In this paper, we have demonstrated a novel new method for determining over-fit, the Ensemble Difference Criterion (EDC), which can be used, for example, on climate data from ensemble simulations. In demanding robustness of the class definitions between different ensemble members, the EDC provides a definitive upper limit on the number of classes supported by the data.

In the example presented here, the GMM classification of Southern Ocean temperature profiles from historical climate simulations of the UK-ESM model, we find that the BIC does not give a strong constraint on over-fitting, and so the EDC is an extremely useful extra tool. Taking into account the information provided by the BIC, the EDC, and Silhouette scores, we find our data can support between four and seven classes.

For reference, we also compare an eight class GMM based on the UK-ESM data with a previous eight class GMM based on Argo observations. We find that there is good agreement between GMMs within the ACC region, however there are too few Argo observations South of the Southern Boundary to provide a good match with the UK-ESM data in this region. Additionally, the sub-tropical classes don't match well between GMMs, either because the simulations don't reproduce the temperature structure of the observed sub-tropical Southern Ocean, or because the temperature profiles are not distinct enough in these regions to support robust classes for an eight class model.

**Acknowledgments.** This work used JASMIN, the UK collaborative data analysis facility. Data analysis was performed using the Pangeo platform, which was supported by NSF Award 1740648.

**Funding Statement.** EB was supported by the NERC grant NE/V013254/1 (ENCORE). DJ was supported by a UKRI Future Leaders Fellowship (MR/T020822/1).

**Competing Interests.** None

**Data Availability Statement.** UKESM1 data are available from the CMIP6 data archive (<https://cmip-pcmdi.llnl.gov/CMIP6/>). Replication data and code for this manuscript can be found at <https://doi.org/10.5281/zenodo.7696487> Boland and Atkinson (2023).

**Ethical Standards.** The research meets all ethical guidelines, including adherence to the legal requirements of the study country.

**Author Contributions.** Conceptualization: D.J.; E.B. Methodology: E.A.; D.J. Data curation: E.B.; E.A. Data visualisation: E.A.; E.B. Writing original draft: E.A.; E.B. All authors approved the final submitted draft.

## References

- Abdi, H. and Williams, L. J. (2010). Principal component analysis. *Wiley interdisciplinary reviews: computational statistics*, 2(4):433–459.
- Akaike, H. (1973). Information Theory and an Extension of the Maximum Likelihood Principle. In Petrov, B. and Caski, F., editors, *Second International Symposium on Information Theory*, pages 267–281, Budapest. Akademiai Kiado.
- Anderson, B. D. and Moore, J. B. (2012). *Optimal filtering*. Courier Corporation.
- Boland, E. and Atkinson, E. (2023). *emmomp/oceanclusteringmethods*: First release.
- Caliński, T. and Harabasz, J. (1974). A dendrite method for cluster analysis. *Communications in Statistics-theory and Methods*, 3(1):1–27.
- Crawford, A. (2020). The Use of Gaussian Mixture Models with Atmospheric Lagrangian Particle Dispersion Models for Density Estimation and Feature Identification. *Atmosphere*, 11(12):1369.
- Davies, D. L. and Bouldin, D. W. (1979). A cluster separation measure. *IEEE Transactions on Pattern Analysis and Machine Intelligence*, PAMI-1(2):224–227.
- Fahrin, F., Jones, D. C., Wu, Y., Keeble, J., and Archibald, A. T. (2022). Unsupervised classification of ozone profiles in ukesm1. *Atmospheric Chemistry and Physics Discussions*, pages 1–27.
- Hannachi, A. (2007). Tropospheric Planetary Wave Dynamics and Mixture Modeling: Two Preferred Regimes and a Regime Shift. *Journal of the Atmospheric Sciences*, 64(10):3521–3541. Publisher: American Meteorological Society Section: Journal of the Atmospheric Sciences.

- Hannachi, A. and O'Neill, A. (2001). Atmospheric multiple equilibria and non-Gaussian behaviour in model simulations. *Quarterly Journal of the Royal Meteorological Society*, 127(573):939–958. \_eprint: <https://onlinelibrary.wiley.com/doi/pdf/10.1002/qj.49712757312>.
- Hjelmervik, K. and Hjelmervik, K. T. (2014). Time-calibrated estimates of oceanographic profiles using empirical orthogonal functions and clustering. *Ocean Dynamics*, 64(5):655–665.
- Hjelmervik, K., Hjelmervik, K. T., and Østenstad, P. (2015). Estimation of oceanographic profiles and climatological regions in the Barents Sea. In *OCEANS 2015 - Genova*, pages 1–6.
- Hjelmervik, K. T. and Hjelmervik, K. (2013). Estimating temperature and salinity profiles using empirical orthogonal functions and clustering on historical measurements Topical Collection on the 16th biennial workshop of the Joint Numerical Sea Modelling Group (JONSMOD) in Brest, France 21–23 May 2012. *Ocean Dynamics*, 63(7):809–821. Publisher: Springer.
- Houghton, I. A. and Wilson, J. D. (2020). El Niño Detection Via Unsupervised Clustering of Argo Temperature Profiles. *Journal of Geophysical Research: Oceans*, 125(9).
- Jones, D. C., Holt, H. J., Meijers, A. J. S., and Shuckburgh, E. (2019). Unsupervised Clustering of Southern Ocean Argo Float Temperature Profiles. *Journal of Geophysical Research: Oceans*, 124(1):390–402.
- Kim, Y. S. and Orsi, A. H. (2014). On the variability of antarctic circumpolar current fronts inferred from 1992–2011 altimetry. *Journal of Physical Oceanography*, 44(12):3054–3071.
- Liu, Y., Chen, W., Chen, Y., Chen, W., Ma, L., and Meng, Z. (2021). Ocean Front Reconstruction Method Based on K-Means Algorithm Iterative Hierarchical Clustering Sound Speed Profile. *JMSE*, 9(11):1233.
- Maze, G., Mercier, H., and Cabanes, C. (2017a). Profile classification models. *Mercator Ocean Journal*, (55):48–56.
- Maze, G., Mercier, H., Fablet, R., Tandeo, P., Lopez Radcenco, M., Lenca, P., Feucher, C., and Le Goff, C. (2017b). Coherent heat patterns revealed by unsupervised classification of Argo temperature profiles in the North Atlantic Ocean. *Progress in Oceanography*, 151:275–292. Publisher: Pergamon.
- Pedregosa, F., Varoquaux, G., Gramfort, A., Michel, V., Thirion, B., Grisel, O., Blondel, M., Prettenhofer, P., Weiss, R., Dubourg, V., Vanderplas, J., Passos, A., Cournapeau, D., Brucher, M., Perrot, M., and Duchesnay, E. (2011). Scikit-learn: Machine learning in Python. *Journal of Machine Learning Research*, 12:2825–2830.
- Rousseeuw, P. J. (1987). Silhouettes: A graphical aid to the interpretation and validation of cluster analysis. *Journal of Computational and Applied Mathematics*, 20:53–65.
- Schwarz, G. (1978). Estimating the dimension of a model. *The annals of statistics*, pages 461–464.
- Sellar, A. A., Jones, C. G., Mulcahy, J. P., Tang, Y., Yool, A., Wiltshire, A., O'connor, F. M., Stringer, M., Hill, R., Palmieri, J., et al. (2019). Ukesm1: Description and evaluation of the uk earth system model. *Journal of Advances in Modeling Earth Systems*, 11(12):4513–4558.
- Solidoro, C., Bandelj, V., Barbieri, P., Cossarini, G., and Fonda Umani, S. (2007). Understanding dynamic of biogeochemical properties in the northern Adriatic Sea by using self-organizing maps and k-means clustering. *Journal of Geophysical Research: Oceans*, 112(C7). \_eprint: <https://onlinelibrary.wiley.com/doi/pdf/10.1029/2006JC003553>.
- Sonnewald, M., Wunsch, C., and Heimbach, P. (2019). Unsupervised Learning Reveals Geography of Global Ocean Dynamical Regions. *Earth and Space Science*, 6(5):784–794. \_eprint: <https://onlinelibrary.wiley.com/doi/pdf/10.1029/2018EA000519>.
- Sugiura, N. (2021). Clustering global ocean profiles according to temperature-salinity structure. arXiv:2103.14165 [physics].
- Tandeo, P., Chapron, B., Ba, S., Autret, E., and Fablet, R. (2014). Segmentation of Mesoscale Ocean Surface Dynamics Using Satellite SST and SSH Observations. *IEEE Trans. Geosci. Remote Sensing*, 52(7):4227–4235.
- Yuchechen, A. E., Lakkis, S. G., Caferri, A., Canziani, P. O., and Muszkats, J. P. (2020). A Cluster Approach to Cloud Cover Classification over South America and Adjacent Oceans Using a k-means/k-means++ Unsupervised Algorithm on GOES IR Imagery. *Remote Sensing*, 12(18):2991.
- Zhao, J., Guo, Z., Guo, Y., Lin, W., and Zhu, W. (2021). A self-organizing forecast of day-ahead wind speed: Selective ensemble strategy based on numerical weather predictions. *Energy*, 218:119509.

Supplementary Figures for: *A Novel Heuristic Method for Detecting  
Overfit in Unsupervised Classification of Climate Models, 2023,*  
Environmental Data Science

Emma J. D. Boland, British Antarctic Survey, Cambridge, United Kingdom.  
Erin Atkinson, University of Toronto, Toronto, Canada.  
Dan(i) Jones, British Antarctic Survey.

### 8 Classes by Ensemble Member

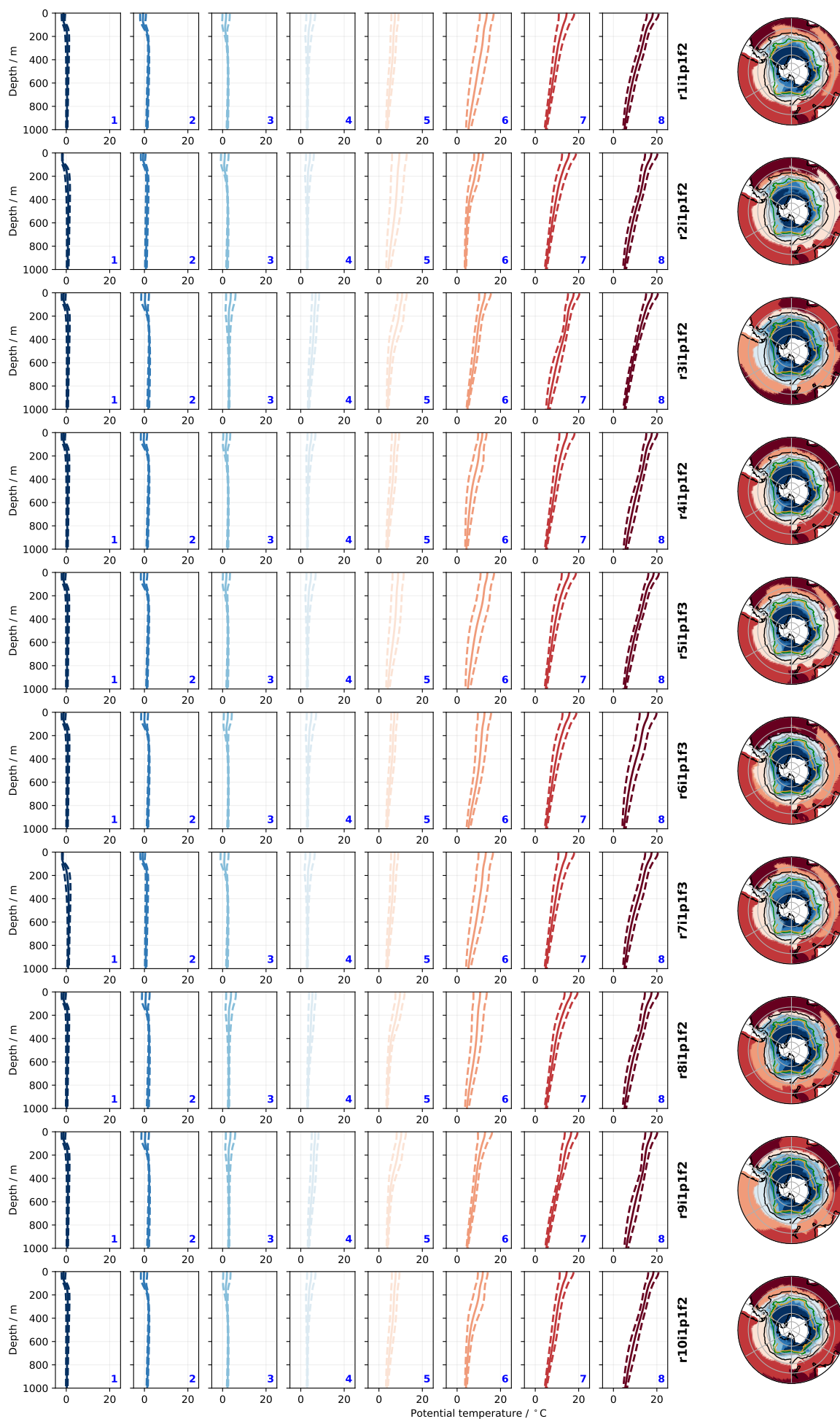


Figure S1: Results of an 8 class Gaussian Mixture Model fit to 2001-2017 Southern Ocean temperature profiles from the UK-ESM CMIP6 historical ensemble, see main manuscript for more details. Each row corresponds to a different ensemble member as labelled. The first eight columns show the time mean and standard deviation

9 Classes by Ensemble Member

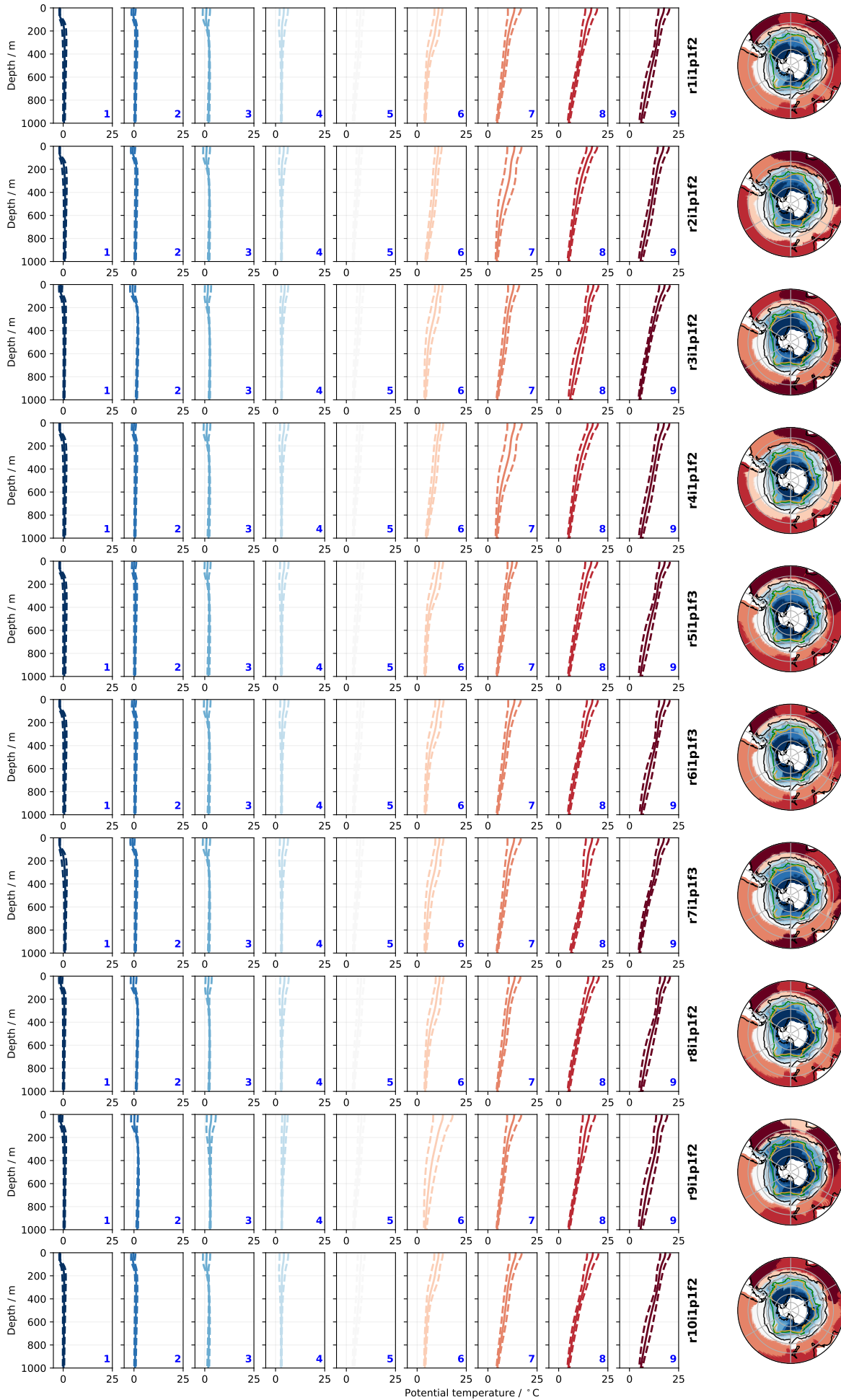


Figure S2: As in figure S1, but for 9 class Gaussian Mixture Model.